



Projectile impact-induced spalling damage on carbon fiber reinforced polymer strengthened RC plates

Huan Tu^{a,c}, Tat Ching Fung^a, Paolo Del Linz^b, Kang Hai Tan^{a,*}

^a School of Civil and Environmental Engineering, Nanyang Technological University, Singapore 639798, Singapore

^b Engineering Cluster, Singapore Institute of Technology, Singapore 138683, Singapore

^c Key Laboratory for Mechanics in Fluid Solid Coupling Systems, Institute of Mechanics, Chinese Academy of Sciences, Beijing, 100190, China

ARTICLE INFO

Keywords:

Projectile impact
CFRP
RC
Spalling damage

ABSTRACT

As the most widely used material in protective structures, a better understanding of the resistance of reinforced concrete (RC) to high-speed projectile striking is needed. It has been accepted that concrete material possesses limited impact resistance in virtue of its poor energy absorption capacity. To improve the performance of RC structures under impulsive loading, affixing externally-bonded Fiber Reinforced Polymer (FRP) sheets on structural elements is a practical method. Due to the emphasis of most existing literature on the penetration behavior of projectiles, the studies of impact-induced spalling damage on normal and FRP strengthened RC plates are not sufficient and in-depth. In this paper, the local response of un-strengthened and FRP strengthened RC plates under projectile impact is systematically investigated with experimental approaches. In consideration of the complexity of transient behavior as well as multiply parameters involved, empirical approaches based on dimensionless analysis are proposed to predict the diameter and depth of spalling craters on normal RC plates and strengthened ones with frontal CFRP layers, which fill current research gap and are potential tools for damage assessment and repair. The validity of the proposed approaches is verified by test results from the present and published studies.

1. Introduction

Due to increasing terrorist attacks and impact incidents, the design of civilian buildings to withstand impact loading has drawn greater attention. The dynamic characteristics and failure modes of structural components have been well elaborated for years [1–3]. In the past few decades, the behavior of reinforced concrete (RC) structures under projectile impacts gradually becomes a research hotspot [4–7]. A major focus of extensive studies is the local response of RC targets caused by hard impact. Li et al. [8] summarized potential damage modes forming on RC plates based on observations from extensive tests as shown in Fig. 1. Three failure modes were observed in the tests: penetration on the impacted face, scabbing on the rear face, and perforation of the whole target [9].

The main concern of existing studies is the depth of penetration (DOP) which is the traveling distance of the projectile into the target and ballistic parameters such as scabbing limit thickness (the minimum thickness of target required to prevent scabbing at the rear face), perforation limit thickness (the minimum thickness of target required to

prevent perforation) and ballistic limit velocity (the minimum impact velocity of a projectile to perforate a target) [9]. Various empirical formulas for quantitative estimation of ballistic effects on concrete structures have been proposed [10–15]. With deeper investigations on damage mechanisms, some semi-analytical models are available. For instance, Forrestal et al. [16] measured the deceleration-time history of the projectile during the penetration and applied Newton's second law to calculate the penetration depth. Besides, the maximum spalling crater depth equal to twice the diameter of projectiles was suggested. Chen and Li [17,18] modified Forrestal et al.'s model basing dimensionless analysis to eliminate dimension inhomogeneity so that it could be applicable to arbitrary projectile nose shape. The majority of existing studies hereinbefore focus on the penetration behavior of impactor. However, the assessment of the protective performance of RC structures should not solely rely on a single parameter DOP. In the design of structures to resist blast loading, the damaged areas on the surfaces of RC elements are of great significance due to potential threats caused by concrete fragments [19–21]. To obtain acceptable predictions on the dynamic response, researchers attempted a variety of approaches to quantitatively analyze the explosion-induced damage and several predictive models were

* Corresponding author.

E-mail address: ckhtan@ntu.edu.sg (K.H. Tan).

<https://doi.org/10.1016/j.compstruct.2023.117129>

Received 20 June 2022; Received in revised form 10 April 2023; Accepted 6 May 2023

Available online 11 May 2023

0263-8223/© 2023 Elsevier Ltd. All rights reserved.

| Nomenclature | | | |
|--------------|---|-------------|--|
| A_c | Spalling crater area on concrete surface | G_{12} | In-plan shear modulus |
| C | Concrete strength-dependent parameter | H_c | Depth of crater depth |
| C_n | FRP layer-dependent parameter | I^* | Dimensionless impact energy |
| d | Diameter of projectile shank | M | Mass of projectile |
| D_c | Equivalent diameter of spalling crater | U | Dimensionless crater volume |
| DOP | Depth of penetration | V | Impact velocity |
| E_1 | Young's modulus in the fiber direction | V_c | Volume of spalling crater |
| E_2 | Young's modulus in the transverse direction | V_{eff} | Effective striking velocity after penetrating FRP |
| E_c | Energy consumed by concrete spalling | α | Corrected parameter for penetration depth |
| E_f | Energy consumed by FRP damage | ν_{12} | Poisson ratio |
| E_k | Kinetic energy of projectile | σ_1 | Tensile strength in the fiber direction |
| f_c | Compressive strength of concrete | σ_2 | Tensile strength transverse to the fiber direction |
| | | τ_{12} | In-plan shear strength |

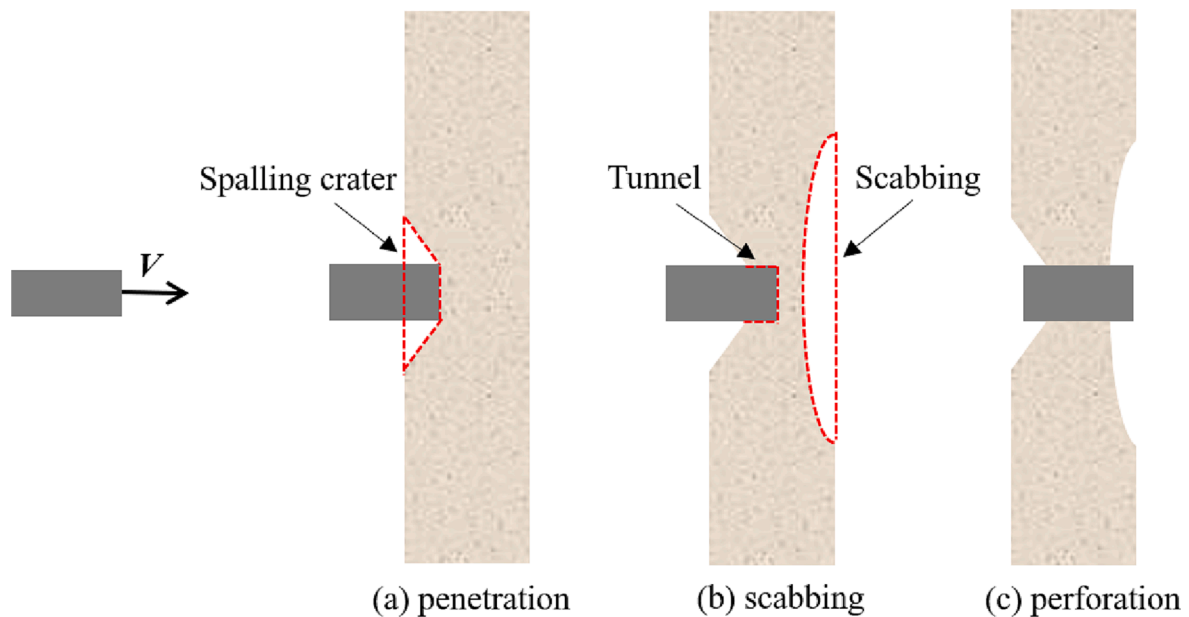


Fig. 1. Projectile impact on the concrete plate (a) penetration; (b) scabbing and (c) perforation.

developed [21–26]. However, the size of projectile impact-induced surface damage on RC components has received less attention, which is required to quantify the extent of damage caused by ejecting small fragments, for instance, for a cased charge. For example, Grisaro and Dancygier [27] estimated the residual resistance of a concrete structure subjected to an explosion basing the material loss. Such analyses, especially when concerned with more sparse impacts, would benefit from a more in-depth study of the surface damage caused by smaller fragments.

It is widely reported that concrete material is vulnerable to dynamic loading, especially when subjected to high-velocity impact and explosion. With increasing requirements for resisting potential threats and accidents, developing practical methods to improve the impact resistance of RC structures is imperative [28]. As mentioned hereinbefore, minimizing surface damage area and preventing projectile perforation are equally important in the design of protective RC plates or panels, as both ways could reduce secondary fragmentation [29]. In this context, with widespread applications of composite materials in the construction industry, externally-bonded fiber-reinforced polymer (FRP) layers have been widely applied to retrofit aging buildings and renovate dilapidated facilities [30–34]. In the past decades, using fiber-reinforced polymer (FRP) sheets as protective layers to strengthen RC structures has gained

increasing popularity due to their superior characteristics, i.e., excellent strength-to-weight ratio, great durability and convenient installation [35]. Except for the mechanical properties of FRP material itself, the bonding strength at the interface [36,37] and the fracture behavior of concrete [38–40] play an important role in the performance of RC structures with externally-bonded FRP layers. In consideration of the catastrophic effects caused by high-velocity impacts, researchers are working to study the dynamic response and failure mechanism of strengthened RC structures in recent years. Vossoughi et al. [41] investigated the behavior of concrete panels protected by Polypropylene and Zylon fabric. Experimental approach was adopted to study the extent of kinetic energy absorbed by concrete targets with and without fabric. As observed from post-impact specimens, scabbing damage on the rear face of concrete panels was reduced and ejection fragments could be prevented by both types of fabric. Abdel-Kader and Fouda [42] conducted a series of projectile impact tests on concrete panels with strengthening Glass Fiber Reinforced Polymer (GFRP) sheets. Similar strengthening effects were reported in which the extent of damage was reduced by FRP sheets. Moreover, the effectiveness of GFRP sheets in reducing spalling damage on the impacted face was elaborated. Almusallam et al. [43] applied experimental and numerical approaches to investigate the dynamic behavior of carbon fiber reinforced polymer

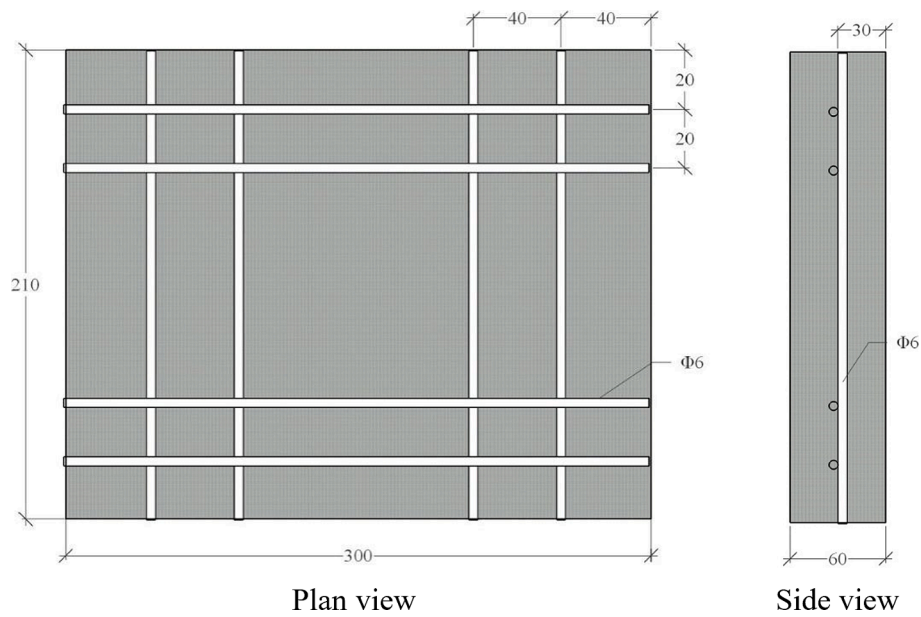


Fig. 2. Reinforcement details of RC plates.

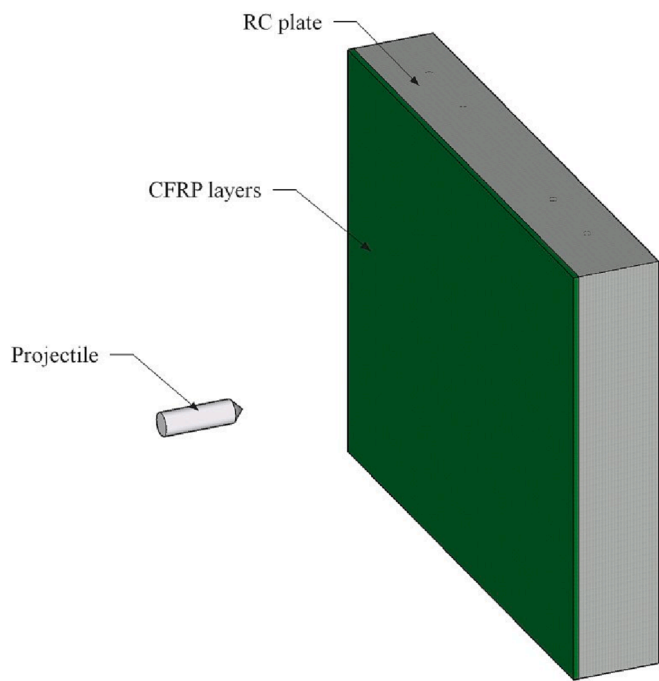


Fig. 3. Schematic diagram of impact test on FRP strengthened RC plate.

Table 2
Mechanical properties of CFRP.

| Property | Definition | Experimental results |
|-------------------|--|----------------------|
| σ_1 (MPa) | Tensile strength in the fiber direction | 750 |
| σ_2 (MPa) | Tensile strength transverse to the fiber direction | 8.3 |
| E_1 (MPa) | Young's modulus in the fiber direction | 83,000 |
| E_2 (MPa) | Young's modulus in the transverse direction | 3700 |
| ν_{12} | Poisson ratio | 0.23 |
| τ_{12} (MPa) | In-plan shear strength | 8.1 |
| G_{12} (MPa) | In-plan shear modulus | 1320 |

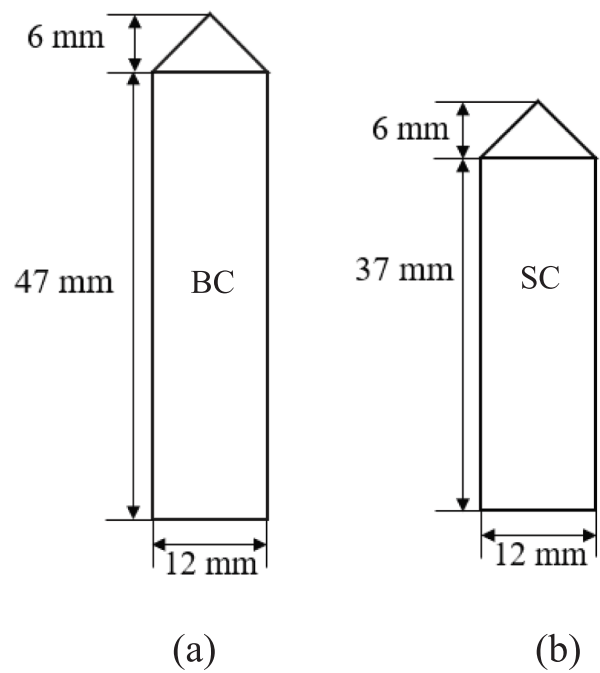


Fig. 4. Geometry of (a) BC (Big-Conical) and (b) SC (Small-Conical) projectiles.

Table 1
Mix proportions of concrete specimens.

| Unconfined compressive strength (MPa) | Cement (kg/m ³) | Fine aggregate (kg/m ³) | Coarse aggregate (kg/m ³) | Water (kg/m ³) | Water/cement ratio |
|---------------------------------------|-----------------------------|-------------------------------------|---------------------------------------|----------------------------|--------------------|
| 25 | 331 | 1014 | 830 | 205 | 0.62 |
| 40 | 465 | 922 | 770 | 243 | 0.52 |
| 50 | 488 | 928 | 759 | 205 | 0.42 |

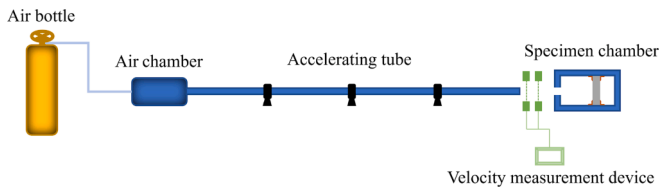


Fig. 5. Sketch of the test setup.

(CFRP) strengthened concrete panels under projectile impact. Localized damage modes including penetration tunnel, crack formation, spalling and scabbing damage and fracture of CFRP sheets were observed. Both impact tests and numerical simulations demonstrated that CFRP sheets could improve perforation energy of concrete panels and prevent fragments flying off the rear face. However, the number of studies on FRP strengthened RC plates under projectile impact is insufficient up till now and the majority of findings rely on qualitative analysis.

In this paper, the local response of normal RC plates and strengthened RC plates with CFRP sheets under hard projectile impact is studied by experimental approach. Since the focus of this study is the spalling damage forming on the impacted face, FRP sheets are attached at the frontal face of RC specimens. As reviewed hereinbefore, there is no available method to predict the size of spalling damage. To fill this gap, an empirical model for RC targets is first proposed. Then a series of tests are conducted for FRP strengthened RC plates. Lastly, a model to evaluate the protection of FRP layers on RC plates is proposed and verified with test results.

2. Experimental program

This study aims to investigate and analyze the spalling damage on the impacted face of normal and FRP strengthened RC plates caused by projectile impact. In comparison of numerical approaches that require sufficient expertise in material properties and impact dynamics as well as extensive computational resource, experimental studies could replicate the actual scenarios and give reliable results in a straightforward manner. Moreover, experiment-based methods are commonly user-friendly to researchers and engineers by incorporating complicated characteristics into specific empirical parameters. Therefore, multiple factors are systematically studied through impact tests, i.e., concrete strength, number of CFRP layers, projectile mass and striking velocity.

2.1. RC plates

The dimensions of RC plates used in the tests were 300 mm × 210 mm × 60 mm. All plates were reinforced with φ6 steel bar along the longitudinal and transverse directions. As the layout of reinforcement shown in Figs. 2 and 3, to prevent the projectile from striking the with rebars, no reinforcement was placed in the central area. The

compressive strength (f_c) of concrete specimens varied from 25 to 50 MPa (cylinder strength at 28 days). Concrete strength was controlled by water/cement (w/c) ratio and the maximum size of coarse aggregate was 10 mm. The w/c ratio used for 25 MPa, 40 MPa and 50 MPa mix was 0.62, 0.52 and 0.42, respectively. The mix proportions of specimens of different concrete grades are shown in Table 1.

2.2. CFRP layers

CFRP layers consist of carbon fiber sheets and matrix material. In this study, unidirectional carbon fiber was selected and the basic properties were provided by the manufacturer. Epoxy resin was used as the matrix material due to its stable performance and good compatibility. To prepare the CFRP strengthened RC plates, epoxy resin was first mixed with the promoter for hardening. Then, the fiber sheets were impregnated by the resin. Before affixing the wet layers onto the RC plates, a thin layer of glue was brushed on the surface of RC plates for better bonding. The prepared specimens were cured at room temperature (26 ~ 30°C) for

Table 3 Experimental plan of RC plates.

| Test group No. | Type of projectile | Concrete grade (MPa) | Gas pressure (MPa) | Repetition | Total number of tests |
|----------------|--------------------|----------------------|--------------------|------------|-----------------------|
| 1 | Small-Conical | 40 | 2 | 3 | 9 |
| | | | 4 | 3 | |
| | | | 6 | 3 | |
| 2 | Big-Conical | 40 | 2 | 3 | 9 |
| | | | 4 | 3 | |
| | | | 6 | 3 | |
| 3 | Big-Conical | 25 | 2 | 3 | 9 |
| | | | 4 | 3 | |
| | | | 6 | 3 | |
| 4 | Small-Conical | 50 | 2 | 3 | 9 |
| | | | 4 | 3 | |
| | | | 6 | 3 | |

Table 4 Experimental plan of CFRP strengthened RC plates.

| Test group No. | Type of projectile | The number of FRP layers | Gas pressure (MPa) | Total number of tests |
|----------------|--------------------|--------------------------|--------------------|-----------------------|
| 1 | Big-Conical | 0 | 2, 4, 6 | 12 |
| | | 1 | 2, 4, 6 | |
| | | 2 | 2, 4, 6 | |
| | | 3 | 2, 4, 6 | |
| 2 | Small-Conical | 0 | 2, 4, 6 | 12 |
| | | 1 | 2, 4, 6 | |
| | | 2 | 2, 4, 6 | |
| | | 3 | 2, 4, 6 | |

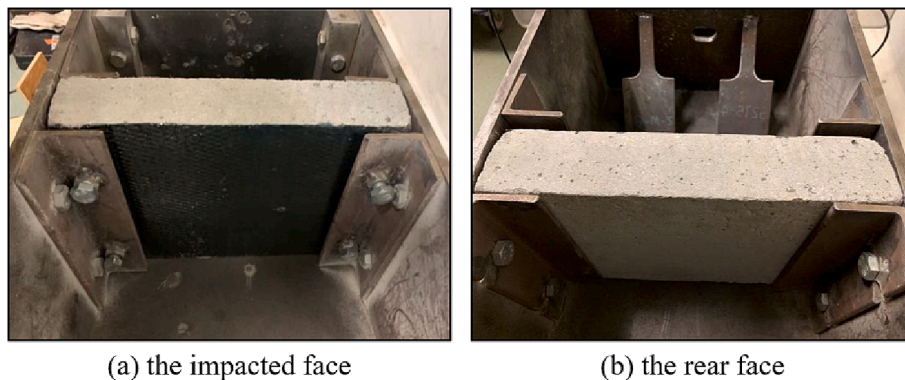
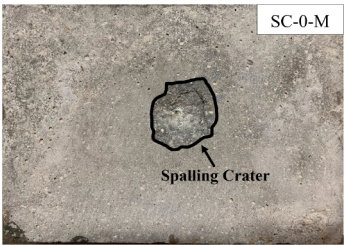
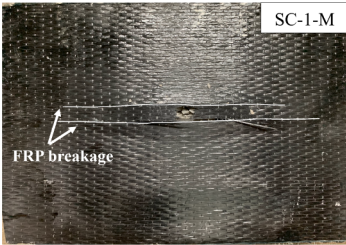
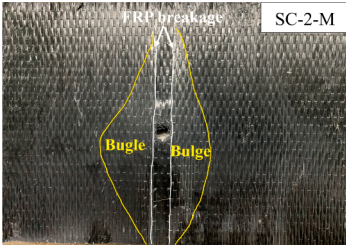
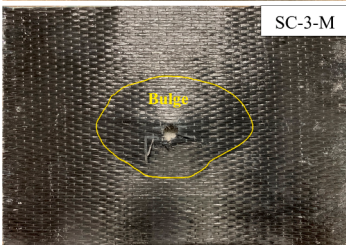


Fig. 6. Fixed specimen in the specimen chamber.

Table 5
Typic damage patterns observed from tests.

| Test specimen | Photos of post-test specimens | Observed damage pattern |
|--------------------------------|--|---|
| Un-strengthened RC plates |  | Spalling crater was formed at the impact point. |
| 1-layer strengthened RC plates |  | (1) FRP layer was perforated by the projectile and a hole was created at the impact point.(2) FRP was fractured along the fiber direction. |
| 2-layer strengthened RC plates |  | (1) FRP layers were perforated by the projectile and a hole was formed at the impact point.(2) The top FRP layer was fractured along the fiber direction.(3) The FRP near the fractured region detached from concrete and bulged. |
| 3-layer strengthened RC plates |  | (1) FRP layers were perforated by the projectile and a hole was formed at the impact point.(2) The FRP near the fractured region detached from concrete and bulged |

one week. The mechanical properties of CFRP layers were tested according to ASTM D 3039 and ASTM D 7565 and the results are summarized in Table 2.

2.3. Projectile

The projectiles used for impact tests were machined from 316 Stainless Steel. Two types of projectiles were designed and prepared, as shown in Fig. 4. All the projectiles were solid and the shank diameter was 12 mm. These two types of projectiles were denoted as BC (Big-Conical) and SC (Small-Conical), respectively. The mass of the BC projectiles was equal to 44.4 g, while the SC projectiles weighted 35 g.

2.4. Setup

In the present impact tests, the projectiles were launched from a 12-mm-diameter gas gun system as shown in Fig. 5. The launching system consisted of an air tank, an air chamber and an accelerating tube. A velocity measurement device located at the exit of the accelerating tube was used to measure the striking velocity of projectiles. Two opposite edges of test specimens were clamped within a chamber, as shown in Fig. 6. The impact velocity was controlled by gas pressure of the air tank and the projectile velocity varied from 100 to 250 mm/ms.

2.5. Experimental program

The entire test program was divided into 2 categorizes, viz., normal RC plates and FRP strengthened RC plates. In the former, specimens made of concrete of different compressive strengths were tested and the aim was to develop a predictive model for RC elements. Furthermore, systematic analysis of RC plates with FRP strengthening layers was conducted based on the results of the second series.

2.5.1. Projectile impact tests on normal RC plates

There were 4 groups of specimens in the first series. In each group, one type of projectiles was used to impact concrete specimens of the same grade. To vary the striking velocity, BC and SC projectiles were accelerated by three pressure levels, viz., low pressure (2 MPa), medium pressure (4 MPa) and high pressure (6 MPa). To guarantee the validity of results, impact tests under one specified pressure level were repeated thrice. Thus, a total of 9 tests were conducted for each group. The whole experimental program is presented in Table 3.

2.5.2. Projectile impact tests on FRP strengthened RC plates

Same to the impact tests for normal RC specimens, two types of projectiles were used in the second series. The concrete strength was kept unchanged, in which all the RC plates were made of C40 concrete. In each group, one specific type of projectile was selected to impact the specimens. The variation of striking velocities was achieved by

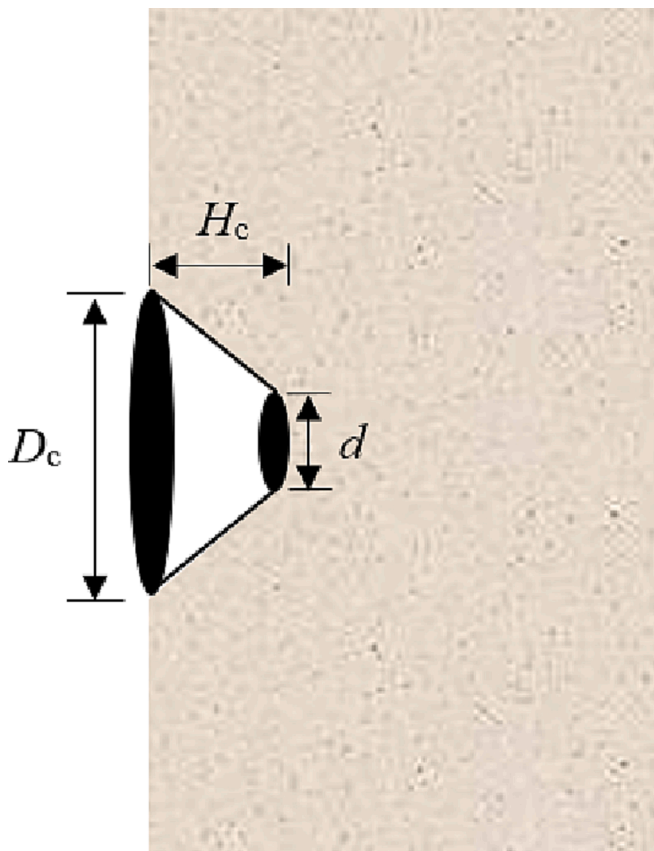


Fig. 7. Frustum-of-cone-shaped spalling crater on the impacted face.

controlling the gas pressure and three levels were applied (2 MPa, 4 MPa and 6 MPa). Moreover, the number of strengthening layers was varied from 0 to 3 to investigate the strengthening effect of FRP sheets. The laminate stacking sequence of 1, 2 and 3 layers was [0], [90/0] and [0/90/0], respectively, where 0° and 90° represented the direction parallel with the longitudinal and transverse directions of the plates, respectively. Thus, each group consisted of 12 individual tests. The whole experimental plan is shown in Table 4.

2.6. Experimental observations

The damage pattern on the post-impact specimen was observed and recorded after each impact. The formation of spalling crater due to concrete crushing was the most common damage mode. Ascribed to the attached FRP layers on the impacted face, the crater could not be observed directly from post-test FRP strengthened specimens. Hence, the initial observation was on externally-bonded FRP sheets. It was found that the damage patterns on the strengthened specimens varied with the number of FRP layers. For specimens with 1 layer of FRP, a hole at the impact point and fractured FRP along fiber direction were observed. The width of damaged region was approximately equal to the diameter of the projectile and the length was changed under different striking velocities. A similar phenomenon was found on the 2-layer strengthened specimens, whereby a through hole was formed on the FRP sheets at the position of impact and the outer layer was torn. In addition, some bulges due to detachment of FRP from the concrete surface were observed. There was no apparent fiber breakage on 3-layer strengthened specimens except subjected to the highest impact velocity. However, a bulging region was found around the impact point. Photos of RC plates and FRP sheets are presented in Table 5 to show the damage patterns.

2.7. Measurements

The aim of experimental studies was to investigate the impact-induced spalling crater. As the most common damage mode caused by projectile impact, simplifying crater model as the frustum of a cone is widely acceptable and such assumption has been verified by tests [44]. As shown in Fig. 7, the authors assume the frustum-of-cone-shaped crater with the ‘base diameter’ as crater diameter D_c and the ‘head diameter’ equal to the projectile shank diameter d . The ‘height’ indicates crater depth H_c . Thus, the volume of spalling crater could be calculated by crater depth H_c , crater diameter D_c and projectile shank diameter d .

The first measurement for post-impact specimens is DOP, measured by a digital caliper. DOPs of all tested plates are smaller than the twice projectile shank diameter ($2d$), which is the maximum spalling crater depth suggested by Forrestal et al. [16]. Thus, the penetration behavior of projectiles could be treated as shallow penetration. Apart from the formation of spalling crater (Fig. 1(a)), other damage modes are not observed (Fig. 1(b) and (c)) and the measured DOP was equal to crater depth H_c . The measurement of crater diameter is not as straightforward as that for DOP due to the irregularity of crater contours. One available method to assess crater diameter D_c is to average the maximum crater diameters in different directions [45,46]. Alternatively, the crater size could be estimated by the diameter of a circle of equal area, also referred to as the equivalent crater diameter. To obtain accurate results, an image processing software Image-Pro Plus was applied in this study. For strengthened specimens, the measurement was conducted followed by the removal of FRP layers. Fig. 8 shows the impacted face of post-impact plate with 1-, 2- or 3-FRP-layer. The enclosed area, namely, spalling crater area A_c , could be calculated by Image-Pro Plus and the corresponding results (values in red area) are shown in each figure. Then the equivalent crater diameter assuming a circular shape could be determined based on the measure crater area by $D_c = \sqrt{\frac{4}{\pi}A_c}$.

3. Analysis of results

3.1. Spalling damage on bare RC plates

The experimental results of normal RC plates are summarized in Table 6. The first column denotes the test number, where four sets of alphabets/digits refer to the type of projectile (BC and SC), the concrete grade, the launching pressure (L- 2 MPa, M-4 MPa and H-6 MPa) and the number of tests, respectively. For example, specimen SC-40-L-01 denotes the first specimen made by concrete with 40 MPa compressive strength subjected to a Small-Conical projectile impact launched by 2 MPa gas pressure.

3.1.1. Analysis of results for normal RC plates

In this series of 36 tests, projectile striking velocity ranged from 100 to 250 m/s. After each impact, only minor abrasions were found on the tip of projectile. Therefore, the deformations of projectiles were deemed to be negligible and all penetration behavior were treated as hard impact, which was consistent with the published experimental observations [17,18]. A spalling crater was observed on all RC plates without obvious scabbing (Fig. 1(a)) on the rear face. Thus, the experimental program was reasonable and met the corresponding demands. As shown in Table 4, DOPs in all the tests were less than 24 mm ($2d$), the maximum spalling crater depth suggested by Forrestal et al [47]. In other words, within the range of tested impact velocities, no tunnels were produced during the penetration of projectiles and it was rational to assume that the impact energy was consumed by RC plates to form spalling craters. Fig. 9 shows the comparison of DOPs between measurements from present tests and semi-analytical predictions by Chen & Li model [17,18]. It was found that the analytical model slightly overestimated DOPs, which might arise from the confinement of reinforcing bars and the influence of coarse aggregates. To quantify the difference, the

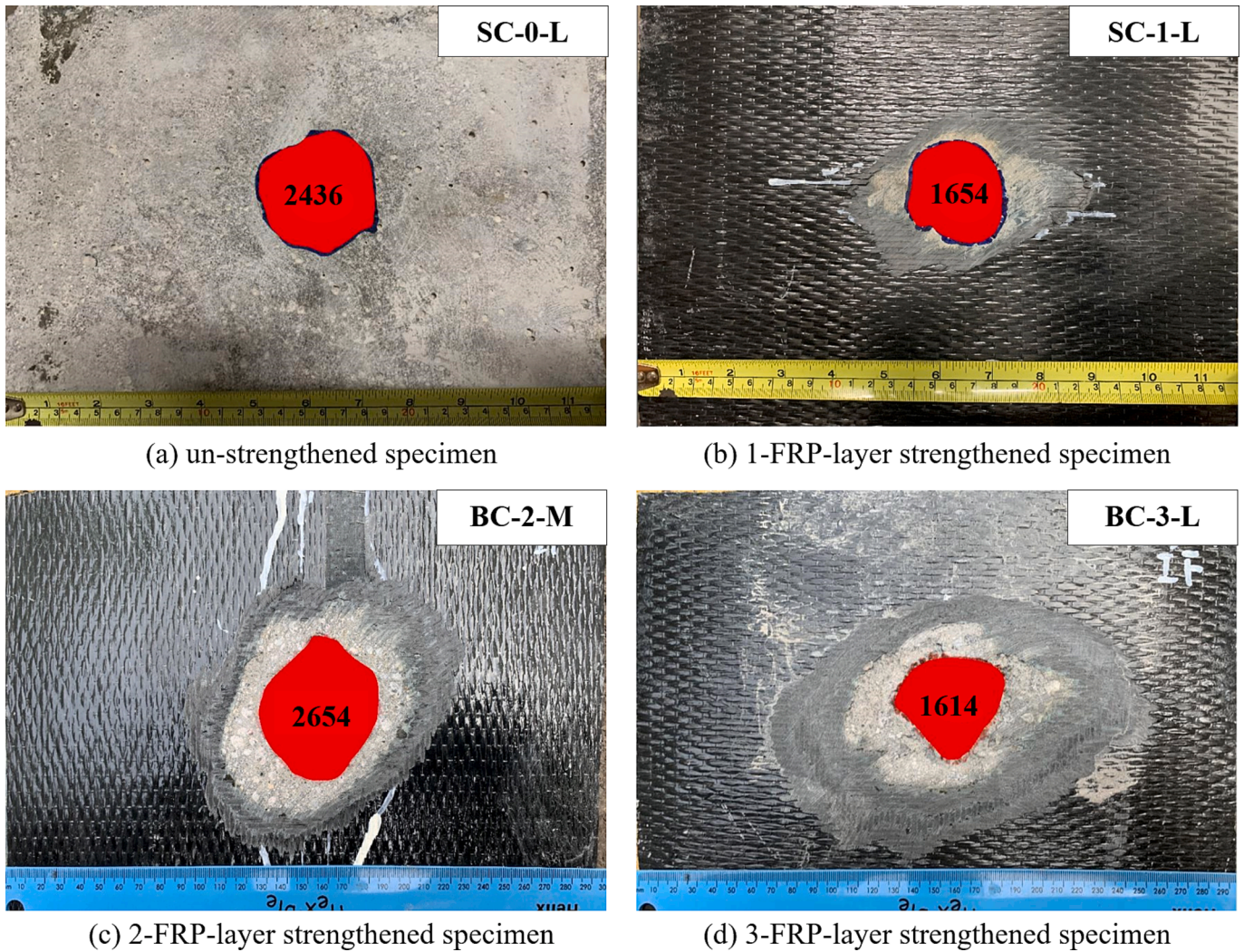


Fig. 8. Measurement of crater area.

average ratio α of semi-analytical predictions to experimental results is calculated and summarized in Table 7, which demonstrates that α is a concrete strength dependent parameter. Thus, the differences between experimental and semi-analytical DOP mainly rely on concrete grades.

3.1.2. Development of the spalling crater predictive model for RC plates

The model for spalling damage prediction is based on the conservation law of energy. During the penetration process, the kinetic energy of the projectile is transferred to the concrete material and is fully consumed by forming an idealized local damage (Fig. 1(a)). A projectile with greater impact energy would cause severer damage. The energy of the rebound projectile is neglected from a conservative perspective. Based on this assumption, total impact energy is converted to producing a spalling crater. Thus, the volume of the spalling crater is assumed to be proportional to the projectile kinetic energy (Eq. (1)).

$$v_c \propto E_k \tag{1}$$

where v_c is the volume of spalling crater and E_k is the kinetic energy of projectile.

The non-dimensional impact factor I^* has been widely used by researchers in their empirical and semi-analytical formulae for DOP calculation [18,48,49]. As shown in Eq. (2), the numerator indicates the kinetic energy of projectile and the denominator represents the impact resistance of target.

$$I^* = \frac{MV^2}{f_c d^3} \tag{2}$$

where M is the mass of projectile, V is the impact velocity, f_c is the concrete compressive strength and d is the shank diameter of projectile.

Based on the frustum-of-cone geometric simplification, the crater volume could be calculated using Eq. (3). To directly compare with the dimensionless parameter I^* , the crater volume v_c was normalized by d^3 to derive parameter U (Eq. (4)).

$$v_c = \frac{1}{12} \pi H_c (D_c^2 + d^2 + D_c d) \tag{3}$$

$$U = \frac{1}{12} \pi \frac{H_c}{d} \left[\left(\frac{D_c}{d} \right)^2 + \frac{D_c}{d} + 1 \right] \tag{4}$$

where H_c is the crater depth (equal to the DOP in this paper); D_c is the crater diameter and d is the shank diameter of projectile. With this formula, the dimensionless crater area A_c/d^2 can be obtained by dividing U by (H_c/d) .

The test results are summarized in an I^* - U plot (Figs. 10 and 11) to show the correlation between two dimensionless parameters. It is found that the normalized crater volume U is linearly proportional to the impact factor I^* . Moreover, the slope is closely associated with concrete compressive strength. Forrestal et al [47] reported that the resistance of

Table 6
Results of projectile impact tests.

| Test no. | Projectile Mass <i>M</i> (g) | Concrete strength <i>f_c</i> (MPa) | Striking velocity <i>V</i> (mm/ms) | DOP (mm) | Crater area <i>A_c</i> (mm ²) | Equivalent crater diameter <i>D_c</i> (mm) |
|------------|------------------------------|--|------------------------------------|----------|---|--|
| SC-40-L-01 | 35 | 40 | 142.31 | 11.82 | 2978.7 | 61.6 |
| SC-40-L-02 | 35 | 40 | 169.38 | 11.88 | 2161.7 | 52.5 |
| SC-40-L-03 | 35 | 40 | 170.07 | 16.05 | 2852.7 | 60.3 |
| SC-40-M-01 | 35 | 40 | 174.09 | 14.75 | 3366 | 65.5 |
| SC-40-M-02 | 35 | 40 | 182.62 | 14.85 | 3500.8 | 66.8 |
| SC-40-M-03 | 35 | 40 | 193.20 | 15.85 | 4114.8 | 72.4 |
| SC-40-H-01 | 35 | 40 | 218.66 | 17.09 | 3938.3 | 70.8 |
| SC-40-H-02 | 35 | 40 | 219.11 | 17.61 | 3128.1 | 63.1 |
| SC-40-H-03 | 35 | 40 | 226.24 | 19.05 | 4038 | 71.7 |
| BC-40-L-01 | 44.4 | 40 | 135.38 | 12.5 | 2902 | 60.8 |
| BC-40-L-02 | 44.4 | 40 | 138.17 | 11.65 | 2354.1 | 54.8 |
| BC-40-L-03 | 44.4 | 40 | 150.91 | 12.02 | 2136.7 | 52.2 |
| BC-40-M-01 | 44.4 | 40 | 151.82 | 12 | 1980 | 50.2 |
| BC-40-M-02 | 44.4 | 40 | 170.07 | 15.13 | 2492 | 56.3 |
| BC-40-M-03 | 44.4 | 40 | 183.37 | 21.25 | 3345 | 65.3 |
| BC-40-H-01 | 44.4 | 40 | 192.80 | 20.25 | 4089.6 | 72.2 |
| BC-40-H-02 | 44.4 | 40 | 203.25 | 21.41 | 5408 | 83.0 |
| BC-40-H-03 | 44.4 | 40 | 219.68 | 20.81 | 5427.6 | 83.2 |
| BC-25-L-01 | 44.4 | 25 | 123.78 | 13.25 | 2017.6 | 50.7 |
| BC-25-L-02 | 44.4 | 25 | 134.72 | 12.97 | 2326.2 | 54.4 |
| BC-25-L-03 | 44.4 | 25 | 135.53 | 12.61 | 3357.5 | 65.4 |
| BC-25-M-01 | 44.4 | 25 | 138.79 | 13.35 | 2353.7 | 54.8 |
| BC-25-M-02 | 44.4 | 25 | 151.21 | 18.85 | 4424.7 | 75.1 |
| BC-25-M-03 | 44.4 | 25 | 178.78 | 21.68 | 4584.2 | 76.4 |
| BC-25-H-01 | 44.4 | 25 | 182.70 | 22.95 | 5349.7 | 82.6 |
| BC-25-H-02 | 44.4 | 25 | 186.38 | 24.65 | 4644.3 | 76.9 |
| BC-25-H-03 | 44.4 | 25 | 195.47 | 22.75 | 3821.6 | 69.8 |
| SC-50-L-01 | 35 | 50 | 145.01 | 10.09 | 1582.1 | 44.9 |
| SC-50-L-02 | 35 | 50 | 162.62 | 10.25 | 3139.3 | 63.2 |
| SC-50-L-03 | 35 | 50 | 168.05 | 11.25 | 2011.3 | 50.6 |
| SC-50-M-01 | 35 | 50 | 168.54 | 13.1 | 3990.1 | 71.3 |
| SC-50-M-02 | 35 | 50 | 169.07 | 14.15 | 2550.1 | 57.0 |
| SC-50-M-03 | 35 | 50 | 184.68 | 15.07 | 2760.9 | 59.3 |
| SC-50-H-01 | 35 | 50 | 200.53 | 16.05 | 2639.4 | 58.0 |
| SC-50-H-02 | 35 | 50 | 209.15 | 17.51 | 3254.9 | 64.4 |
| SC-50-H-03 | 35 | 50 | 215.95 | 19.28 | 4169.9 | 72.9 |

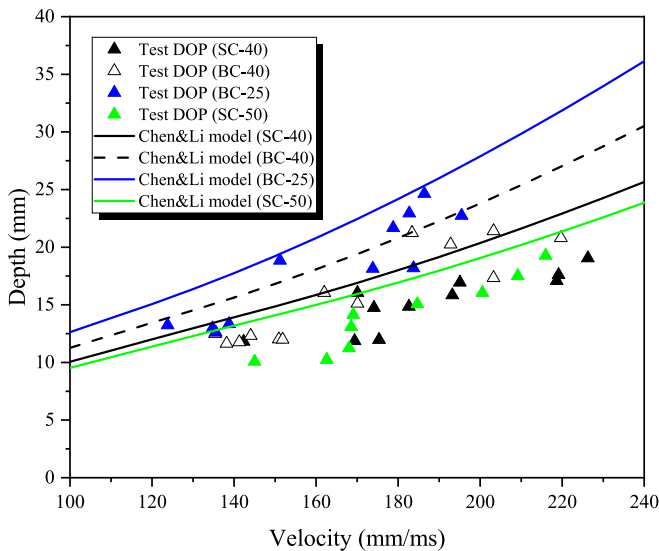


Fig. 9. Comparison between test results and Chen & Li model predictions.

concrete targets to projectile impacts is highly governed by concrete strength. They introduced a strength-dependent parameter *S* in their model. In this study, an experimental parameter *C* that represents the slope of fitting lines in Fig. 9a-c is proposed and thus the projectile impact-induced spalling crater could be directly obtained through Eq.

Table 7

The average ratio of semi-analytical results to experimental results (α).

| Test group | Number of tests | α |
|------------|-----------------|----------|
| BC-25 | 9 | 1.18 |
| BC-40 | 9 | 1.24 |
| SC-40 | 9 | 1.24 |
| SC-50 | 9 | 1.3 |

(5). The term *C* is a concrete strength-dependent parameter and it is equal to 0.637, 0.71 and 0.767 for *f_c* = 25 MPa, 40 MPa and 50 MPa concrete, respectively.

$$U = C \times I^* \tag{5}$$

With the empirical parameter *C*, the dimensionless crater volume *U* could be determined according to the impact factor *I**. Then Chen & Li model for the calculation of normalized crater depth (*H_c/d*) is incorporated. The normalized crater diameter *D_c/d* could be evaluated using Eq. (6).

$$\frac{D_c}{d} = \frac{-1 + \sqrt{1 - 4 \left(1 - \frac{12CId}{\pi H_c}\right)}}{2} \tag{6}$$

3.1.3. Verification

The accuracy of the proposed approach to predict crater diameter is firstly verified by the present test results. Eq. (7) is slightly modified by introducing the parameter α to eliminate the overestimation of DOPs by

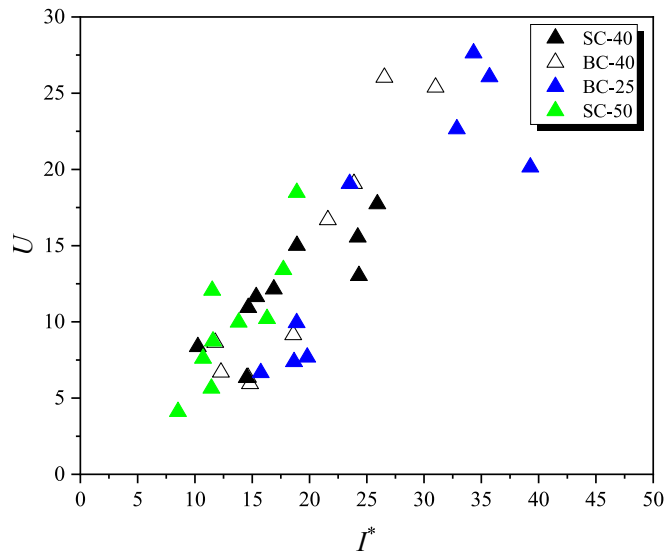


Fig. 10. Relationship between dimensionless crater volume U and impact factor I^* .

Chen & Li model. The comparison between experimental results and predictions is summarized in Table 8. To better present the differences,

prediction errors are plotted in Fig. 12. As clearly presented in the chart, the errors of all predictions are less than 20% and most of them are within 10% difference, which indicate good predictive capability of the proposed approach.

$$\frac{D_c}{d} = \frac{-1 + \sqrt{1 - 4 \left(1 - \frac{12\alpha C I d}{\pi H_c} \right)}}{2} \tag{7}$$

The proposed approach is also verified by published test data [50–52] and the corresponding comparisons are shown in Table 9. Reasonable predictions on the referenced test results are obtained through the proposed approach. The maximum error (-19.89%) is found in Jeongsoo Nam et al.’s test [51]. A possible reason to produce such a difference might be that the researchers used a spherical projectile in their tests. The predicted crater diameters of Beppu et al. [50] and Kojima [52] tests are close to the measured results, with errors of -10.47% and 4.23%, respectively.

3.2. Spalling damage on FRP strengthened RC plates

The measurement data of all 24 specimens is summarized in Table 10, in which the first column indicates the test number. In the nomenclature for specimens, three sets of alphabets/digits refer to the type of projectile (BC and SC), the number of FRP layers and the gas pressure (L- 2 Mpa, M-4 Mpa and H-6 Mpa). For example, SC-1-L

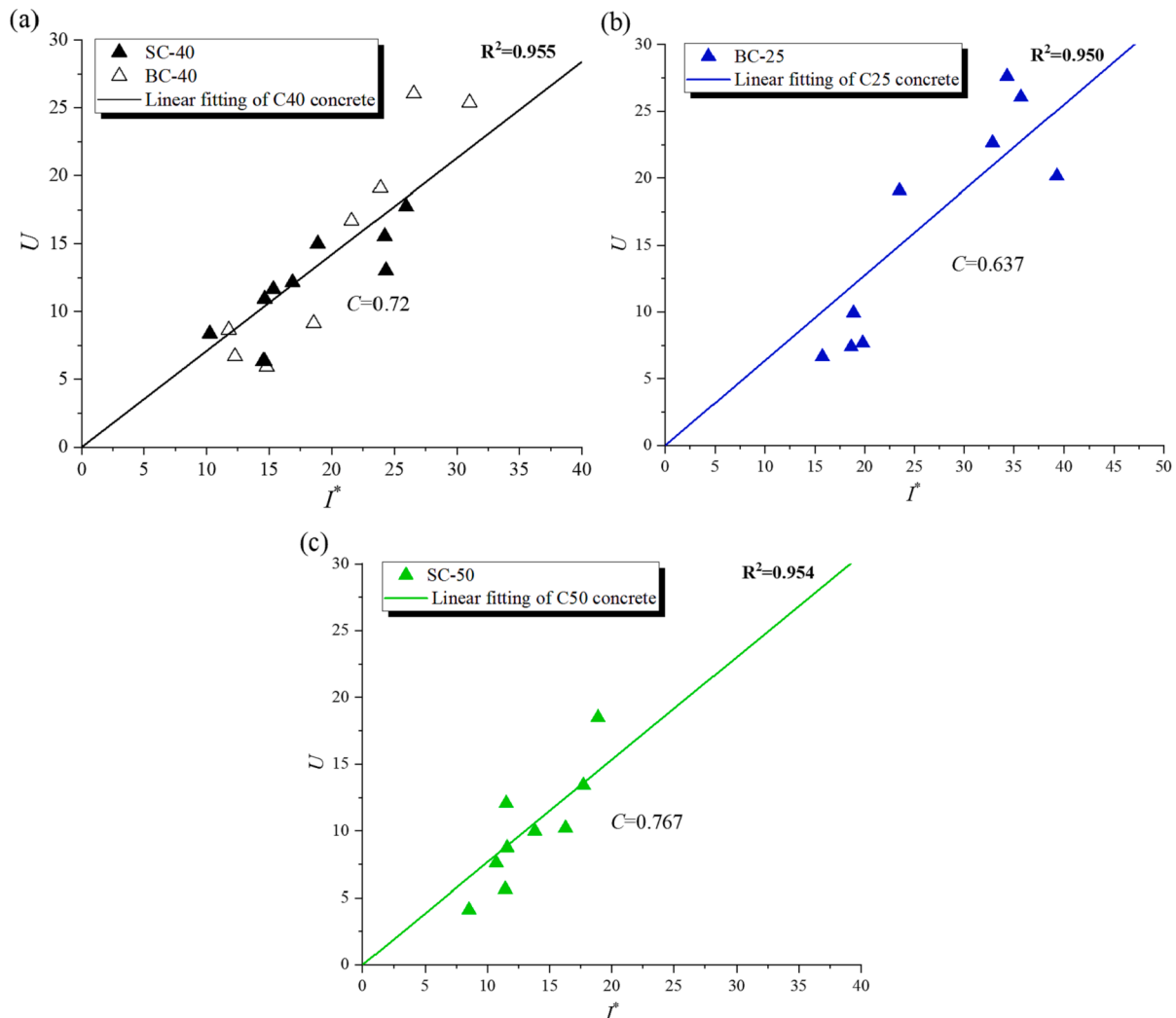


Fig. 11. Linear fitting of data points of different concrete grades (a) C40; (b) C25 and (c) C50.

Table 8
Comparison of crater diameter between tests and predictions.

| Test no. | I^* | C | α | $\frac{H_c}{d}$ | $\left(\frac{D_c}{d}\right)_{Model}$ | $\left(\frac{D_c}{d}\right)_{Test}$ | Error |
|------------|-------|-------|----------|-----------------|--------------------------------------|-------------------------------------|---------|
| SC-40-L-01 | 10.26 | 0.72 | 1.24 | 1.18 | 4.84 | 5.13 | -6.03% |
| SC-40-L-02 | 14.52 | 0.72 | 1.24 | 1.40 | 5.34 | 4.37 | 18.07% |
| SC-40-L-03 | 14.65 | 0.72 | 1.24 | 1.41 | 5.35 | 5.02 | 6.08% |
| SC-40-M-01 | 15.35 | 0.72 | 1.24 | 1.45 | 5.41 | 5.46 | -0.81% |
| SC-40-M-02 | 16.89 | 0.72 | 1.24 | 1.53 | 5.54 | 5.57 | -0.43% |
| SC-40-M-03 | 18.90 | 0.72 | 1.24 | 1.63 | 5.69 | 6.03 | -6.06% |
| SC-40-H-01 | 24.21 | 0.72 | 1.24 | 1.90 | 6.00 | 5.90 | 1.59% |
| SC-40-H-02 | 24.31 | 0.72 | 1.24 | 1.90 | 6.00 | 5.26 | 12.37% |
| SC-40-H-03 | 25.92 | 0.72 | 1.24 | 1.98 | 6.08 | 5.98 | 1.69% |
| BC-40-L-01 | 11.77 | 0.72 | 1.24 | 1.26 | 5.04 | 5.07 | -0.53% |
| BC-40-L-02 | 12.26 | 0.72 | 1.24 | 1.29 | 5.10 | 4.56 | 10.49% |
| BC-40-L-03 | 14.63 | 0.72 | 1.24 | 1.41 | 5.34 | 4.35 | 18.61% |
| BC-40-M-01 | 14.81 | 0.72 | 1.24 | 1.42 | 5.36 | 4.19 | 21.89% |
| BC-40-M-02 | 18.58 | 0.72 | 1.24 | 1.62 | 5.65 | 4.70 | 16.97% |
| BC-40-M-03 | 21.60 | 0.72 | 1.24 | 1.77 | 5.84 | 5.44 | 6.87% |
| BC-40-H-01 | 23.88 | 0.72 | 1.24 | 1.89 | 5.96 | 6.01 | -0.91% |
| BC-40-H-02 | 26.54 | 0.72 | 1.24 | 2.03 | 6.08 | 6.92 | -13.72% |
| BC-40-H-03 | 31.00 | 0.72 | 1.24 | 2.25 | 6.25 | 6.93 | -10.79% |
| BC-25-L-01 | 15.75 | 0.637 | 1.18 | 1.30 | 5.34 | 4.22 | 20.95% |
| BC-25-L-02 | 18.65 | 0.637 | 1.18 | 1.42 | 5.59 | 4.54 | 18.80% |
| BC-25-L-03 | 18.88 | 0.637 | 1.18 | 1.43 | 5.60 | 5.45 | 2.74% |
| BC-25-M-01 | 19.80 | 0.637 | 1.18 | 1.47 | 5.67 | 4.56 | 19.52% |
| BC-25-M-02 | 23.50 | 0.637 | 1.18 | 1.62 | 5.90 | 6.26 | -6.03% |
| BC-25-M-03 | 32.85 | 0.637 | 1.18 | 2.00 | 6.32 | 6.37 | -0.78% |
| BC-25-H-01 | 34.31 | 0.637 | 1.18 | 2.06 | 6.37 | 6.88 | -7.99% |
| BC-25-H-02 | 35.70 | 0.637 | 1.18 | 2.11 | 6.42 | 6.41 | 0.11% |
| BC-25-H-03 | 39.27 | 0.637 | 1.18 | 2.25 | 6.53 | 5.81 | 10.89% |
| SC-50-L-01 | 8.52 | 0.767 | 1.3 | 1.14 | 4.77 | 3.74 | 21.58% |
| SC-50-L-02 | 10.71 | 0.767 | 1.3 | 1.27 | 5.10 | 5.27 | -3.27% |
| SC-50-L-03 | 11.44 | 0.767 | 1.3 | 1.31 | 5.20 | 4.22 | 18.84% |
| SC-50-M-01 | 11.51 | 0.767 | 1.3 | 1.32 | 5.21 | 5.94 | -14.13% |
| SC-50-M-02 | 11.58 | 0.767 | 1.3 | 1.32 | 5.21 | 4.75 | 8.92% |
| SC-50-M-03 | 13.82 | 0.767 | 1.3 | 1.45 | 5.46 | 4.94 | 9.50% |
| SC-50-H-01 | 16.29 | 0.767 | 1.3 | 1.59 | 5.68 | 4.83 | 14.95% |
| SC-50-H-02 | 17.72 | 0.767 | 1.3 | 1.67 | 5.79 | 5.37 | 7.33% |
| SC-50-H-03 | 18.89 | 0.767 | 1.3 | 1.74 | 5.87 | 6.07 | -3.44% |

denotes a specimen strengthened with 1 FRP layer subjected to a SC projectile impact launched by 2 Mpa gas pressure.

3.2.1. Analysis of results for strengthened RC plates

The impact velocity of projectiles varied from 100 to 250 mm/ms. Based on the observation after each strike, no significant deformation was found on projectiles and the penetration behavior of projectiles could be regarded as hard impact. Since no obvious scabbing or cracks were observed on the rear face of plates, concrete spalling and the FRP fracture/deformation are two dominant damage modes on specimens. The measured DOP less than 24 mm (2d) confirmed that projectiles did not produce tunnels during the penetration process and the entire kinetic energy was consumed by causing spalling crater and FRP damage.

In this series of tests, FRP sheets were affixed on the impacted face of RC plates as sacrificial layers to absorb a part of impact energy. In theory, externally-bonded FRP layers could reduce the damage on the protected targets. For clarity, all measured DOPs are summarized and plotted in Fig. 13. Meanwhile, DOPs predicted by Chen & Li model for un-strengthened concrete plates are also presented to directly show the differences between semi-analytical and experimental results. It is worth noting that the penetration depth of projectiles into RC plates with FRP sheets is smaller than that into normal RC plates. In BC test groups, increasing the number of FRP layers is effective to resist the projectile and the penetration depth is reduced significantly. The effectiveness of FRP sheets is also observed in the tests using SC projectiles.

Spalling crater area on each post-impact specimen is measured and the results are presented in Fig. 14. It is clearly shown that the crater area on the impacted face of RC plates is inversely proportional to the number of affixed FRP layers. In comparison with normal specimens, the reduction of crater area on strengthened RC plates is significant,

especially when 2 and 3 layers of FRP sheets are used. Since the FRP sheets are made of unidirectional fiber bundles that possess the highest mechanical performance in the fiber orientation with relatively low tensile strength in the transverse direction, 2 FRP layers in [0°/90°] stacking sequence could constrain deformations and enhance mechanical performance in the transverse direction. Further increasing the number of FRP layers from 2 to 3 lead to minor improvements, where

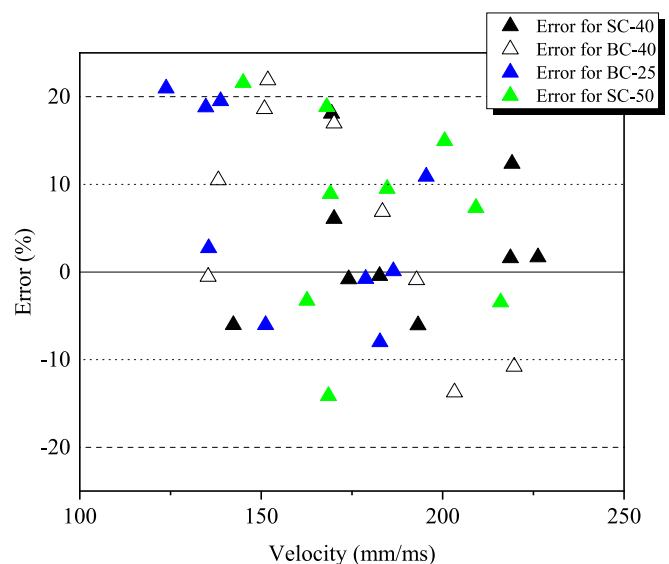


Fig. 12. Errors of predicted spalling diameters.

Table 9
Comparisons between referenced test results and predictions.

| | Projectile | | Concrete strength f_c (MPa) | Striking velocity V (m/s) | $\left(\frac{D_c}{d}\right)_{Model}$ | $\left(\frac{D_c}{d}\right)_{Test}$ | Error |
|--------------------------|---------------|--------------|-------------------------------|-----------------------------|--------------------------------------|-------------------------------------|---------|
| | Nose shape | Mass M (g) | | | | | |
| Beppu et al. [50] | Hemispherical | 50 | 25 | 195.47 | 3.62 | 4.00 | -10.47% |
| Kojima [52] | Hemispherical | 2000 | 27.5 | 209.00 | 5.40 | 5.17 | 4.23% |
| Jeongsoo Nam et al. [51] | Spherical | 35 | 55.2 | 161.00 | 4.95 | 5.94 | -19.89% |

Table 10
Results of projectile impact tests.

| Test no. | Projectile | | Number of FRP layers | Striking velocity V (mm/ms) | DOP (mm) | Crater area A_c (mm ²) | Equivalent crater diameter D_c (mm) |
|----------|------------|--------------|----------------------|-------------------------------|----------|--------------------------------------|---------------------------------------|
| | Nose shape | Mass M (g) | | | | | |
| BC-0-L | Conical | 44.4 | 0 | 140.90 | 13.46 | 2692.3 | 58.6 |
| BC-0-M | Conical | 44.4 | 0 | 185.64 | 20.67 | 3674.6 | 68.4 |
| BC-0-H | Conical | 44.4 | 0 | 195.31 | 23.79 | 3833 | 69.9 |
| BC-1-L | Conical | 44.4 | 1 | 133.71 | 13.27 | 2114.1 | 51.9 |
| BC-1-M | Conical | 44.4 | 1 | 200.00 | 20.1 | 3325.9 | 65.1 |
| BC-1-H | Conical | 44.4 | 1 | 205.48 | 22.41 | 3110.2 | 62.9 |
| BC-2-L | Conical | 44.4 | 2 | 143.87 | 11.24 | 1591.1 | 45.0 |
| BC-2-M | Conical | 44.4 | 2 | 176.47 | 17.44 | 2635.8 | 57.9 |
| BC-2-H | Conical | 44.4 | 2 | 229.78 | 21.8 | 3347.7 | 65.3 |
| BC-3-L | Conical | 44.4 | 3 | 158.23 | 12.63 | 1613.9 | 45.3 |
| BC-3-M | Conical | 44.4 | 3 | 211.86 | 18.91 | 2993.7 | 61.8 |
| BC-3-H | Conical | 44.4 | 3 | 213.68 | 19.51 | 2921.6 | 61.0 |
| SC-0-L | Conical | 35 | 0 | 139.46 | 9.2 | 2436.3 | 55.7 |
| SC-0-M | Conical | 35 | 0 | 169.41 | 14.46 | 2784.7 | 59.6 |
| SC-0-H | Conical | 35 | 0 | 229.57 | 16.16 | 3809.9 | 69.7 |
| SC-1-L | Conical | 35 | 1 | 145.01 | 10.2 | 1654 | 45.9 |
| SC-1-M | Conical | 35 | 1 | 199.95 | 15.75 | 2919.9 | 61.0 |
| SC-1-H | Conical | 35 | 1 | 228.66 | 17.5 | 3299.5 | 64.8 |
| SC-2-L | Conical | 35 | 2 | 149.73 | 10.2 | 1512.7 | 43.9 |
| SC-2-M | Conical | 35 | 2 | 193.05 | 16.98 | 1812 | 48.0 |
| SC-2-H | Conical | 35 | 2 | 245.58 | 22.42 | 2559.3 | 57.1 |
| SC-3-L | Conical | 35 | 3 | 138.40 | 9.48 | 1512.7 | 43.9 |
| SC-3-M | Conical | 35 | 3 | 170.22 | 14.04 | 1812 | 48.0 |
| SC-3-H | Conical | 35 | 3 | 262.51 | 17.28 | 2559.3 | 57.1 |

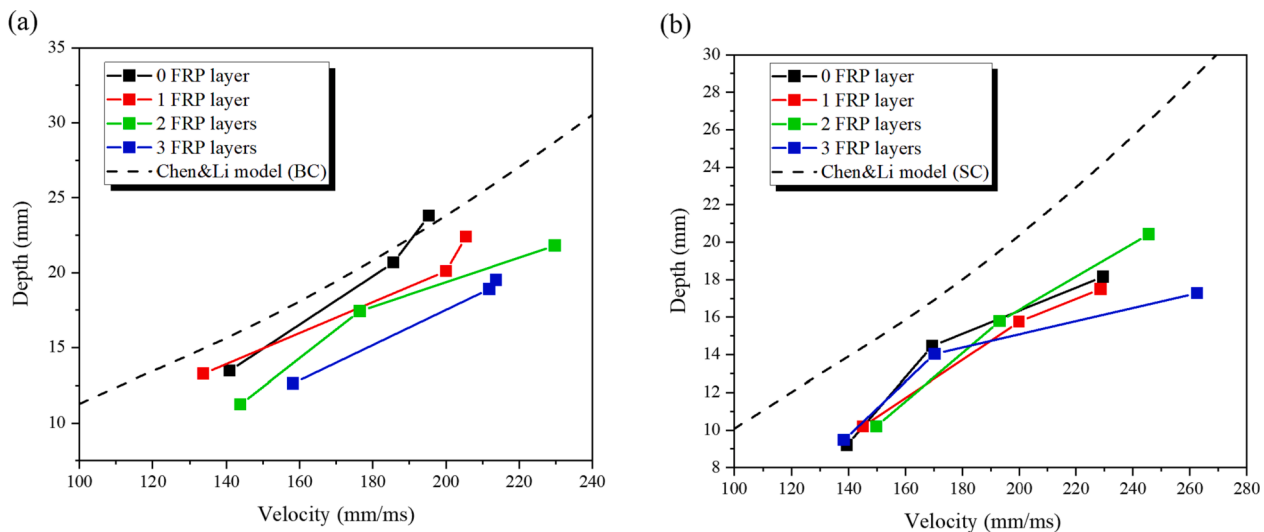


Fig. 13. DOP induced by (a) BC and (b) SC projectiles.

the crater area on RC plates with 2 and 3 FRP layers is close, as shown in Fig. 14.

3.2.2. Development of the spalling crater predictive model for strengthened RC plates

Based on the test results, frontal strengthening FRP layers could protect RC targets and reduce spalling damages. To quantify the rein-

forcing effect of FRP sheets, dimensionless analysis is conducted to establish the relations among key parameters. A critical assumption made in this study is that the impact energy is fully consumed to produce spalling crater and FRP damage. Hence, a formula (Eq. (8)) based on the law of energy conservation is proposed.

$$E_k = E_f + E_c \tag{8}$$

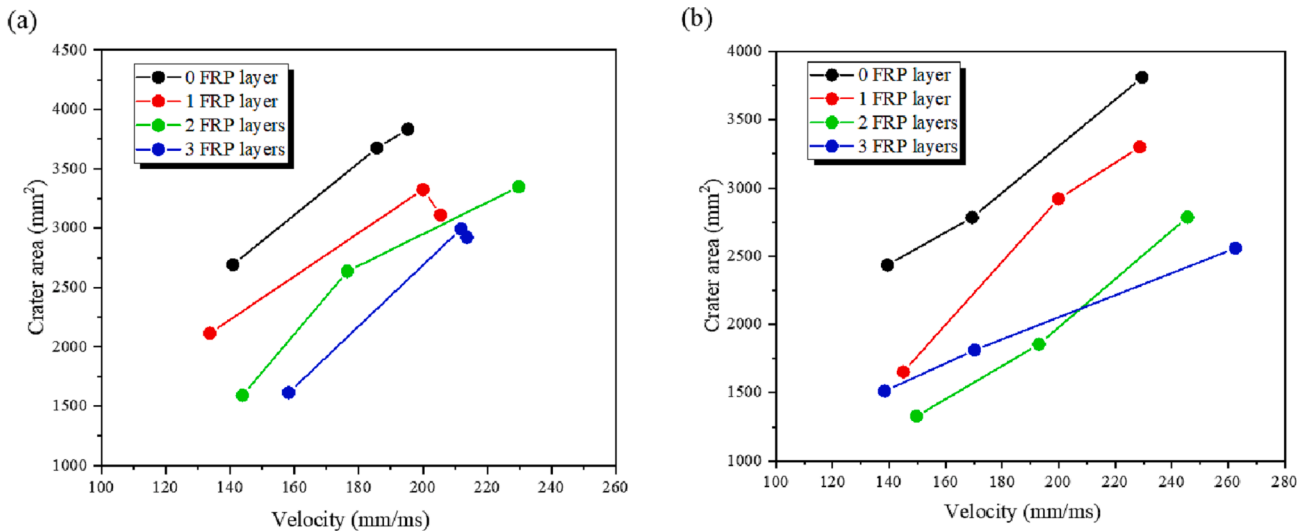


Fig. 14. Crater area induced by (a) BC and (b) SC projectiles.

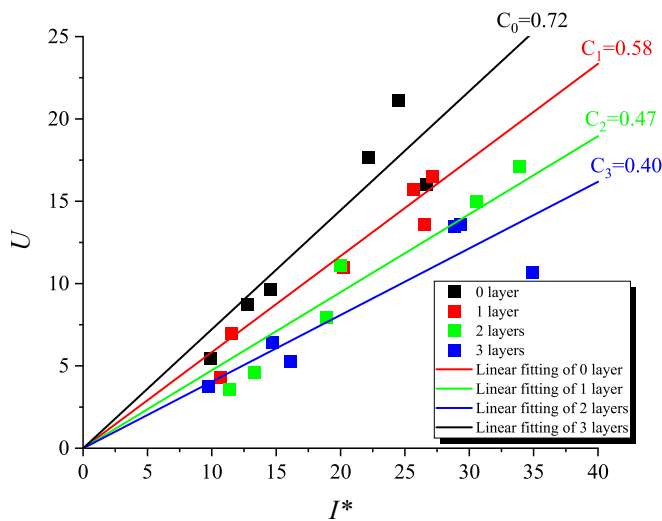


Fig. 15. Relationship between dimensionless crater volume U and impact factor I^* .

Table 11
Calculations of the ratio of C for FRP strengthened specimens.

| Projectile | Specimen | C_n | C_n/C_0 |
|------------|-------------------------------------|-------|-----------|
| Conical | Control specimens | 0.72 | 100% |
| | 1 FRP layer strengthened specimens | 0.58 | 81% |
| | 2 FRP layers strengthened specimens | 0.47 | 65% |
| | 3 FRP layers strengthened specimens | 0.40 | 56% |

where E_k is the projectile kinetic energy, E_f and E_c are the energy consumed by FRP damage and concrete spalling, respectively, and v_c is the volume of spalling crater.

Two parameters I^* and U present dimensionless impact energy and dimensionless crater volume, respectively, which have been introduced in Section 3.1.2. Following the same analysis approach, test results of FRP strengthened specimens are processed and summarized in the I^* - U plot (Fig. 15). As the data points shown in Fig. 15, U is proportional to I^* and the relationship could be approximated to a linear variation. Therefore, four linear fitting lines are proposed for RC plates with 0–3 FRP strengthening layers to indicate the dependence of U on I^* . The

correlation coefficient (R^2) of fitting lines is greater than 0.96, demonstrating the great linearity between these two parameters. The slope of each line C varies with the layer number. It is worth noting that the slope of the fitting line of the control group is identical to the obtained results in Section 3.1. The repeatable results confirm that C is indeed a representative material-dependent parameter. For strengthened RC plates with 1, 2 and 3 FRP layers, C is 0.56, 0.50 and 0.42, respectively. The reduction of values indicate that smaller spalling crater is formed on the RC targets if more FRP layers are affixed on the impacted face. To quantify the improvement effect of externally-bonded layers, the parameter C of FRP strengthened specimens is compared with that of unstrengthened ones. The ratio of C (C_n/C_0 , $n = 1, 2$ and 3) reflects the proportion of impact energy effectively acting on RC plates to cause spalling damage. As the calculations shown in Table 11, 19%, 35% and 44% of the impact energy is absorbed by 1, 2 and 3 FRP strengthening layers, respectively.

To modify the empirical method proposed in Section 3.1 by introducing the improvement effect of strengthening layers, the spalling damage on RC plates with frontal FRP layers can be quantitatively assessed. Based on the ratio of C in Table 11, the impact energy consumed by FRP sheets could be determined and the effective impact velocity striking on the strengthened RC targets could be calculated by Eq. (9). As an example, a projectile with velocity V impacting on a 1-FRP-layer strengthened RC plate, the effective impact velocity V_{eff} acting on the RC target was equal to $(81\%)^{0.5}V = 0.9 V$. Therefore, the calculation of spalling depth and diameter should be based on the effective velocity rather than the original value. By introducing the ratio of C to consider the energy loss on frontal FRP layers, the proposed model can predict the size of spalling crater on FRP strengthened RC plates.

$$\frac{1}{2}MV_{eff}^2 = \frac{C_n}{C_0}E_k \tag{9}$$

where M is the mass of projectile, V_{eff} is the effective striking velocity of projectile acting on RC plates, C_n is the experimental factor of RC plate with n strengthening layers (not more than 3) and E_k is the total kinetic energy of projectile.

3.2.3. Verification

The comparison between the test results and the predictions by the modified method is summarized in Table 12. Moreover, the errors are presented in Fig. 16 to clearly show the accuracy of predictions. The proposed model provides reasonable estimations of both crater depth

Table 12
Comparison of DOP and crater diameter between test results and predictions.

| Test no. | V (mm/ms) | $\sqrt{\frac{C_m}{C_0}}$ | V_{eff} (mm/ms) | I^* | C | $\left(\frac{DOP}{d}\right)_{Model}$ | $\left(\frac{DOP}{d}\right)_{Test}$ | Error | $\left(\frac{D_c}{d}\right)_{Model}$ | $\left(\frac{D_c}{d}\right)_{Test}$ | Error |
|----------|----------------|--------------------------|----------------------|-------|------|--------------------------------------|-------------------------------------|-------|--------------------------------------|-------------------------------------|-------|
| BC-0-L | 139.46 | 1.00 | 139.46 | 9.85 | 0.71 | 1.16 | 0.77 | 34% | 6.19 | 4.64 | 3% |
| BC-0-M | 169.41 | 1.00 | 169.41 | 14.53 | 0.71 | 1.39 | 1.21 | 13% | 6.75 | 4.96 | 8% |
| BC-0-H | 229.57 | 1.00 | 229.57 | 26.69 | 0.71 | 1.83 | 1.35 | 26% | 7.40 | 5.81 | 10% |
| BC-1-L | 145.01 | 0.91 | 131.96 | 8.82 | 0.71 | 1.10 | 0.85 | 23% | 5.17 | 3.83 | 17% |
| BC-1-M | 199.95 | 0.91 | 181.95 | 16.76 | 0.71 | 1.48 | 1.31 | 11% | 5.31 | 5.08 | 9% |
| BC-1-H | 228.66 | 0.91 | 208.08 | 21.92 | 0.71 | 1.68 | 1.46 | 13% | 6.56 | 5.40 | 11% |
| BC-2-L | 149.73 | 0.81 | 121.28 | 7.45 | 0.71 | 1.03 | 0.85 | 17% | 4.58 | 3.66 | 16% |
| BC-2-M | 193.05 | 0.81 | 156.37 | 12.38 | 0.71 | 1.29 | 1.42 | -10% | 5.44 | 4.00 | 22% |
| BC-2-H | 245.58 | 0.81 | 198.92 | 20.04 | 0.71 | 1.61 | 1.87 | -16% | 6.29 | 4.76 | 20% |
| BC-3-L | 138.40 | 0.75 | 103.80 | 5.46 | 0.71 | 0.92 | 0.79 | 14% | 4.30 | 3.66 | 6% |
| BC-3-M | 170.22 | 0.75 | 127.67 | 8.25 | 0.71 | 1.07 | 1.17 | -9% | 5.04 | 4.00 | 11% |
| BC-3-H | 262.51 | 0.75 | 196.88 | 19.63 | 0.71 | 1.59 | 1.44 | 10% | 5.70 | 4.76 | 19% |
| SC-0-L | 149.76 | 1.00 | 149.76 | 8.27 | 0.71 | 1.08 | 0.90 | 17% | 5.59 | 4.44 | 2% |
| SC-0-M | 170.26 | 1.00 | 170.26 | 10.70 | 0.71 | 1.20 | 1.23 | -2% | 6.01 | 4.86 | 1% |
| SC-0-H | 200.75 | 1.00 | 200.75 | 14.87 | 0.71 | 1.40 | 1.24 | 11% | 6.75 | 4.88 | 10% |
| SC-1-L | 149.76 | 0.91 | 136.29 | 6.85 | 0.71 | 1.00 | 0.92 | 8% | 4.56 | 4.50 | -7% |
| SC-1-M | 170.26 | 0.91 | 154.94 | 8.86 | 0.71 | 1.11 | 1.03 | 7% | 4.95 | 4.78 | -4% |
| SC-1-H | 200.75 | 0.91 | 182.69 | 12.31 | 0.71 | 1.28 | 1.25 | 3% | 5.51 | 4.99 | 3% |
| SC-2-L | 149.16 | 0.81 | 120.82 | 5.39 | 0.71 | 0.92 | 0.60 | 35% | 4.47 | 3.26 | 15% |
| SC-2-M | 170.26 | 0.81 | 137.91 | 7.02 | 0.71 | 1.01 | 1.03 | -2% | 4.81 | 3.66 | 14% |
| SC-2-H | 200.75 | 0.81 | 162.61 | 9.76 | 0.71 | 1.15 | 1.22 | -6% | 5.43 | 3.96 | 17% |
| SC-3-L | 146.20 | 0.75 | 109.65 | 4.44 | 0.71 | 0.87 | 0.62 | 29% | 4.03 | 3.52 | 1% |
| SC-3-M | 170.26 | 0.75 | 127.70 | 6.02 | 0.71 | 0.96 | 1.03 | -8% | 4.35 | 4.08 | -2% |
| SC-3-H | 215.05 | 0.75 | 161.29 | 9.60 | 0.71 | 1.14 | 1.36 | -19% | 4.91 | 4.17 | 12% |

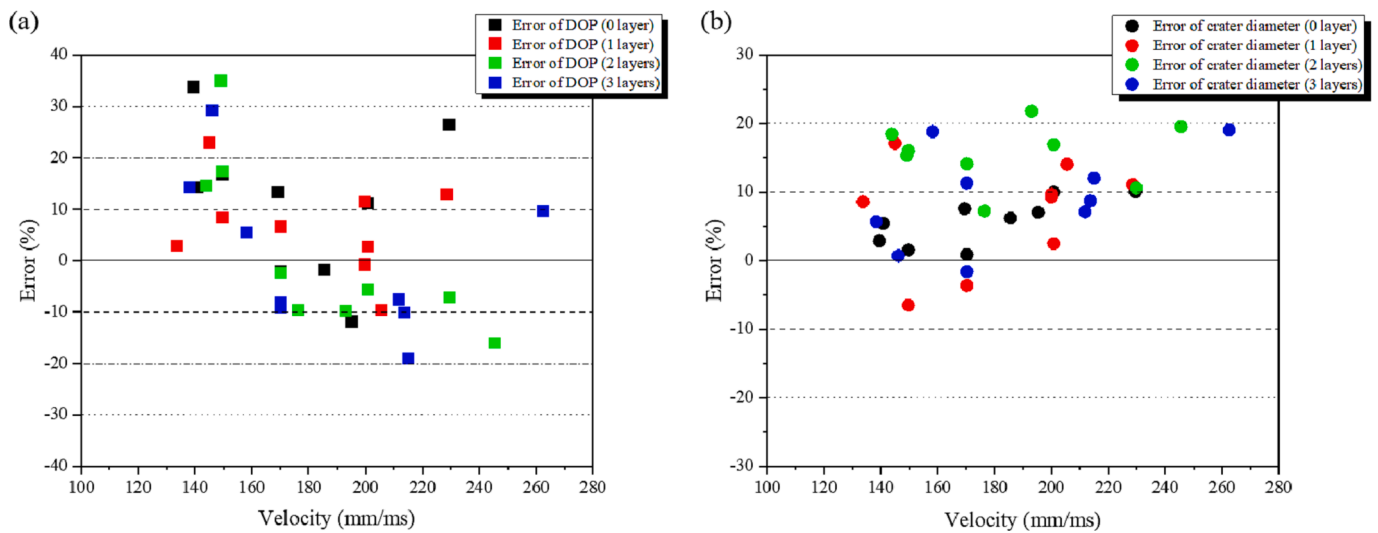


Fig. 16. Prediction errors of (a) DOP and (b) crater diameter.

and diameter. The differences between experimental and predicted DOPs in most of the tests are within 20% except for two cases (BC-0-L and SC-2-L). In terms of crater diameter evaluation, except for 22% overestimation in BC-2-M, all other tests were well predicted with errors lower than 20%. Therefore, this modified empirical approach is capable to predict the size of spalling crater on FRP strengthened RC plates.

4. Conclusion

In this study, to systematically investigate the effects of multiply factors on projectile impact-induced damage, normal RC plates made of three grades of concrete ($f_c = 25, 40$ and 50 MPa) and strengthened RC plates with FRP sheets [(number of layers varying from 1 to 3)] were tested with different impact velocities [ranging from 100 to 250 mm/ms]. The authors propose prediction approaches for both normal and FRP strengthened RC plates basing dimensionless analysis of the test results, which lead to that the size of spalling damage on protected

structural components could be quantitatively evaluated. The main theories and assumptions used for developing the models are summarized as follows:

- Crater is in a frustum-of-cone shape.
- Penetration depth should be shallow (DOP less than $2d$) and only a spalling crater formed on concrete targets.
- The crater depth is determined semi-analytically by Chen & Li model [17,18].
- Dimensionless parameters I^* and U are approximated in a linear relationship and the slope factor C was derived by linearly fitting the test results to the proposed formula.

Since the dynamic behavior of structural components under projectile impact is transient and complex, the theoretical analysis of damage formation is of great difficulty. Moreover, the current studies on the impact-induced spalling damage of FRP strengthened RC plates are not

sufficient and in-depth, which leads to the lack of damage evaluation models. Based on the empirical parameter C obtained in the present paper, the relationship between the impact energy and the volume of spalling crater is directly established and thus the localized damage on normal and strengthened RC plates could be determined in a fast and convenient method. The developed model is potentially to be a practical tool for engineers to design, assess and reinforce RC structures to resist impact effects. The validity of the approach proposed in predicting spalling crater on normal and FRP strengthened RC plates is verified by test results from the present and published studies.

Data availability

The raw/processed data required to reproduce these findings cannot be shared at this time as the data also forms part of an ongoing study.

CRedit authorship contribution statement

Huan Tu: Methodology, Validation, Investigation, Data curation, Writing – original draft. **Tat Ching Fung:** Writing – review & editing, Supervision, Funding acquisition. **Paolo Del Linz:** Conceptualization, Formal analysis, Data curation. **Kang Hai Tan:** Writing – review & editing, Supervision, Funding acquisition.

Declaration of Competing Interest

The authors declare that they have no known competing financial interests or personal relationships that could have appeared to influence the work reported in this paper.

Data availability

The raw/processed data required to reproduce these findings cannot be shared at this time as the data also forms part of an ongoing study.

References

- [1] Darban H, et al. Higher modes of buckling in shear deformable nanobeams. *Int J Eng Sci* 2020;154:103338.
- [2] Tocci Monaco G, et al. Hygro-thermal vibrations and buckling of laminated nanoplates via nonlocal strain gradient theory. *Compos Struct* 2021;262:113337.
- [3] Bossio A, et al. Simplified Model for Strengthening Design of Beam-Column Internal Joints in Reinforced Concrete Frames. *Polymers* 2015;7(9):1732–54.
- [4] Belov NN, et al. ANALYSIS OF REINFORCED-CONCRETE STRENGTH UNDER IMPACT LOADING. *J Appl Mech Tech Phys* 2006;47(6):911–7.
- [5] Dancygier AN, Yankelevsky DZ, Jaegermann C. Response of high performance concrete plates to impact of non-deforming projectiles. *Int J Impact Eng* 2007;34(11):1768–79.
- [6] Distler P, Sadegh-Azar H, Heckotter C. Enhancement of engineering models for simulation of soft, and hard projectile impact on reinforced concrete structures. *Nuclear Eng Des* 2021:378.
- [7] Lu G, Li XB, Wang KJ. A numerical study on the damage of projectile impact on concrete targets. *Comput Concr* 2012;9(1):21–33.
- [8] Li Q, et al. Local impact effects of hard missiles on concrete targets. *Int J Impact Eng* 2005;32(1–4):224–84.
- [9] Fang Q, Wu H. Concrete structures under projectile impact. In: *Concrete Structures Under Projectile Impact*. Springer; 2017. p. 497–558.
- [10] Pétry, *Monographies de systemes d'artillerie*. 1910.
- [11] Beth, R., *Penetration of projectiles in concrete*. PPAB Interim Report, Washington, DC, 1941.
- [12] Gwaltney, R.C., *MISSILE GENERATION AND PROTECTION IN LIGHT-WATER-COOLED POWER REACTOR PLANTS*. 1968, Oak Ridge National Lab., Tenn.
- [13] ACE, *Fundamentals of protective design*. 1946, Army Corps of Engineers, Office of the Chief of Engineer.
- [14] NDRC, O., *Effects of impact and explosion*. 1946, National Defense Research Committee Washington, DC.
- [15] Kar AK. Local effects of tornado-generated missiles. *J Struct Div* 1978;104(5):809–16.
- [16] Forrestal M, et al. Penetration of concrete targets with deceleration-time measurements. *Int J Impact Eng* 2003;28(5):479–97.
- [17] Chen X, Li Q. Deep penetration of a non-deformable projectile with different geometrical characteristics. *Int J Impact Eng* 2002;27(6):619–37.
- [18] Li Q, Chen X. Dimensionless formulae for penetration depth of concrete target impacted by a non-deformable projectile. *Int J Impact Eng* 2003;28(1):93–116.
- [19] UFC 3-340-02, *Structures to resist the effects of accidental explosions*, in *US Department of the Army, Navy and Air Force Technical Manual*. 2008.
- [20] Beppu M, et al. Contact explosion resistance of concrete plates externally strengthened with FRP laminates. *Int J Protect Struct* 2010;1(2):257–70.
- [21] McVay, M.K., *Spall damage of concrete structures*. 1988, ARMY Engineer Waterways Experiment Station Vicksburg MS Structures LAB.
- [22] Morishita M, et al. Damage of reinforced concrete slabs subjected to contact detonations. *J Struct Eng A* 2000;46:1787–97.
- [23] Gebbeken, N., et al. *The engineering-tool XploSim to determine the effects of explosive loadings on reinforced and fibre reinforced concrete structures*. in *Proc. of 18th Int. Symp. Military Aspects of Blast and Shock*. 2004.
- [24] Remennikov A, Mentus I, Uy B. Explosive breaching of walls with contact charges: theory and applications. *Int J Protect Struct* 2015;6(4):629–47.
- [25] Tu H, et al. An analytical model to predict the compressive damage of concrete plates under contact detonation. *Int J Impact Eng* 2019;134:103344.
- [26] Tu H, et al. An analytical model to predict spalling and breaching of concrete plates under contact detonation. *Int J Impact Eng* 2022;160:104075.
- [27] Grisaro H, Dancygier AN. Representation of damage caused by fragmentation impact in design and analysis of reinforced concrete barriers. *Eng Struct* 2019;197:109387.
- [28] Krauthammer, T., *Modern protective structures*. Vol. 22. 2008: CRC Press.
- [29] Grisaro H, Dancygier AN. Assessment of the perforation limit of a composite RC barrier with a rear steel liner to impact of a non-deforming projectile. *Int J Impact Eng* 2014;64:122–36.
- [30] Brena SF, McGuirk GN. Advances on the Behavior Characterization of FRP-Anchored Carbon Fiber-Reinforced Polymer (CFRP) Sheets Used to Strengthen Concrete Elements. *Int J Concrete Struct Mater* 2013;7(1):3–16.
- [31] Lee D, Shin A-H-C. Finite element study on the impact responses of concrete masonry unit walls strengthened with fiber-reinforced polymer composite materials. *Compos Struct* 2016;154:256–68.
- [32] Jin L, et al. Numerical analysis of the mechanical behavior of the impact-damaged RC beams strengthened with CFRP. *Compos Struct* 2021;274:114353.
- [33] Buchan PA, Chen JF. Blast resistance of FRP composites and polymer strengthened concrete and masonry structures – A state-of-the-art review. *Compos B Eng* 2007;38(5):509–22.
- [34] Cantwell W, Smith K. The static and dynamic response of CFRP-strengthened concrete structures. *J Mater Sci Lett* 1999;18(4):309–10.
- [35] Pham TM, Hao H. Review of concrete structures strengthened with FRP against impact loading. *Structures*. Elsevier; 2016.
- [36] Bruno D, et al. Multi-layer modeling of edge debonding in strengthened beams using interface stresses and fracture energies. *Eng Struct* 2016;109:26–42.
- [37] Obaidat YT, Heyden S, Dahlblom O. The effect of CFRP and CFRP/concrete interface models when modelling retrofitted RC beams with FEM. *Compos Struct* 2010;92(6):1391–8.
- [38] De Maio U, et al. A refined diffuse cohesive approach for the failure analysis in quasibrittle materials—part I: Theoretical formulation and numerical calibration. *Fatigue Fract Eng Mater Struct* 2020;43(2):221–41.
- [39] Greco F, Leonetti L, Luciano R. A multiscale model for the numerical simulation of the anchor bolt pull-out test in lightweight aggregate concrete. *Constr Build Mater* 2015;95:860–74.
- [40] De Maio U, et al. Investigation of concrete cracking phenomena by using cohesive fracture-based techniques: A comparison between an embedded crack model and a refined diffuse interface model. *Theor Appl Fract Mech* 2021;115:103062.
- [41] Vossoughi F, et al. Resistance of concrete protected by fabric to projectile impact. *Cem Concr Res* 2007;37(1):96–106.
- [42] Abdel-Kader MM, Fouda A. Improving the impact resistance of concrete panels by glass fiber reinforced polymer sheets. *Int J Protect Struct* 2017;8(2):304–20.
- [43] Almusallam T, et al. Effect of CFRP strengthening on the response of RC slabs to hard projectile impact. *Nucl Eng Des* 2015;286:211–26.
- [44] Hwang H-J, Kim S, Kang TH. Energy-based penetration model for local impact-damaged concrete members. *ACI Struct J* 2017;114(5):1189.
- [45] Abdel-Kader M, Fouda A. Effect of reinforcement on the response of concrete panels to impact of hard projectiles. *Int J Impact Eng* 2014;63:1–17.
- [46] Wu H, et al. Hard projectile perforation on the monolithic and segmented RC panels with a rear steel liner. *Int J Impact Eng* 2015;76:232–50.
- [47] Forrestal M, et al. An empirical equation for penetration depth of ogive-nose projectiles into concrete targets. *Int J Impact Eng* 1994;15(4):395–405.
- [48] Chang WS. Impact of solid missiles on concrete barriers. *J Struct Div* 1981;107(2):257–71.
- [49] Hughes G. Hard missile impact on reinforced concrete. *Nucl Eng Des* 1984;77(1):23–35.
- [50] Beppu M, et al. Damage evaluation of concrete plates by high-velocity impact. *Int J Impact Eng* 2008;35(12):1419–26.
- [51] NAM, J., et al., *IMPACT RESISTANT PERFORMANCE OF DUCTILE FIBER REINFORCED CEMENTITIOUS COMPOSITES (DFRCCs)*.
- [52] Kojima I. An experimental study on local behavior of reinforced concrete slabs to missile impact. *Nucl Eng Des* 1991;130(2):121–32.